Research Article Vol. 28, No. 5 / 2 March 2020 / Optics Express 7116
Optics EXPRESS

Laser induced thermoelastic surface displacement in solids detected simultaneously by photothermal mirror and interferometry

G. A. S. Flizikowski,[1] O. A. Capeloto,[1] V. G. Camargo,[1] B. Anghinoni,[1] M. L. Baesso,[1] L. C. Malacarne,[1] M. P. Belançon,[2] T. Požar,[3] and N. G. C. Astrath[1,*]

[1]Departamento de Física, Universidade Estadual de Maringá, Maringá, PR 87020-900, Brazil
[2]Universidade Tecnológica Federal do Paraná, Pato Branco, PR 85503-390, Brazil
[3]Faculty of Mechanical Engineering, University of Ljubljana, Ljubljana 1000, Slovenia
*ngcastrath@uem.br

Abstract: We propose a combined pump-probe optical method to investigate heat diffusion properties of solids. We demonstrate single-shot simultaneous laser-induced thermoelastic surface displacement of metals detected by concurrent measurements using photothermal mirror and interferometry. Both methods probe the surface displacement by analyzing the wavefront distortions of the probe beams reflected from the surface of the sample. Thermoelastic properties are retrieved by transient analysis in combination with numerical description of the thermoelastic displacement and temperature rise in the sample and in the surrounding air. This technique presents a capability for material characterization that can be extended to experiments for quantitative surface mapping.

© 2020 Optical Society of America under the terms of the OSA Open Access Publishing Agreement

1. Introduction

All-optical pump-probe methods are advanced techniques for general non-destructive material characterization, characterized by detecting the effects generated by the interaction between light and matter. These effects depend on the ability of the material to convert light into radiative and non-radiative processes [1].

The non-contacting nature of pump-probe methods allows accessing thermal, optical and mechanical properties of solids. These methods require reflective surfaces in order to directly detect the perturbation caused by light absorption and have to be capable of detecting probe beam wavefront deformation. Two such methods are the photothermal mirror and the interferometry [2–7]. Both are naturally similar in this sense, because they detect wavefront distortion, although employing different optical detection mechanisms.

The photothermal mirror (TM) spectrometry detects the deformation of the illuminated surface by analyzing the focusing or defocusing of the reflected probe beam in the far field region [8–12]. TM measures a convoluted signal arising from the wavefront distortion caused by the probed surface of the sample in addition to the phase shift created by heat-coupling in the fluid surrounding the sample. This method has been recently introduced under pulsed Gaussian laser excitation for the measurement of thermal diffusivity and thermo-optical properties of semi-transparent and opaque solids [8,9] and for the detection of thermoelastic waves launched by a localized heat deposition [13–15]. This method has also been used to detect surface displacements induced by radiation pressure at air-liquids interfaces [11,12].

Out-of-plane surface displacement can be detected with a homodyne quadrature laser interferometer (HQLI) [16–18], a special extension of the arm-compensated Michelson interferometer [18,19]. HQLI employs the quadrature detection using a stable, linearly polarized laser. Using an additional octadic-wave plate and a polarizing beam splitter, two orthogonally polarized

#386344 https://doi.org/10.1364/OE.386344
Journal © 2020 Received 19 Dec 2019; revised 10 Feb 2020; accepted 10 Feb 2020; published 25 Feb 2020

Optics EXPRESS

interference signals in phase quadrature are generated and detected by two photodiodes. These two signals provide the means to measure the displacements with a sub-nanometer resolution, high dynamic range and constant sensitivity. This method has been used to detect laser-induced, out-of-plane point displacements of high-amplitude and high-frequency [18,20]. The HQLI also senses the phase shift induced by the thermal lens, the underlying effect used in refractometers [21].

In this paper, we present a combined pump-probe method to detect laser induced thermoelastic surface displacement in metals by simultaneous measurement using photothermal mirror and interferometry. A single-shot continuous wave excitation laser beam is used to induce surface displacement of the sample by heat generation following surface optical absorption. Heat propagates to the surrounding air changing its refractive index with temperature creating a thermal lens effect in the air. Both methods probe the surface displacement of the sample and the thermal lens effect in the fluid by analyzing wavefront distortions of the probe beams reflected from the surface of the sample. The interferometer senses the out-of-plane surface displacement and the thermal lens effect at a single location on the surface, while the photothermal mirror senses the total laser induced phase shift caused on the surface of the sample and in the surrounding air. The theoretical predictions are quantitative and describe the experiments performed in metals. We demonstrate the utility of this combined technique to detect thermoelastic displacement at the nanometer-scale. The single-shot combined method has revealed important features that a single technique could not discern with the same precision, including features such as heat diffusion properties as well as mechanical perturbations.

2. Theory

The detection methods use two probe beams and a single excitation beam. The cw Gaussian (TEM_{00}) laser beam propagates along the z-axis and excites the sample almost perpendicular to its surface. The sample surface is located at $z = 0$. Part of the laser power is absorbed at the sample surface and converted into heat, and the rest is reflected. By conduction, heat is transferred to the surrounding air generating a thermal lens due to the temperature dependence of the refractive index of air. Due to the circular symmetric geometry of the problem, the scalar temperature and the vector displacement fields depend only on the normal z- and radial r-coordinates.

The spatiotemporal distribution of the temperature change, $T_i(r, z, t)$, is solved for the sample ($i = s$) and for the surrounding fluid ($i = f$), which obeys the heat diffusion equation [9]

$$\frac{\partial T_i(r,z,t)}{\partial t} - D_i \nabla^2 T_i(r,z,t) = \zeta Q_0 Q(r) Q(z), \tag{1}$$

where $\zeta = 1$ for $i = s$ and $\zeta = 0$ for $i = f$. For the Gaussian beam excitation, $Q(r) = \exp(-2r^2/w_e^2)$ and $Q_0 = 2P_e(1-R)\phi/\pi c_s \rho_s w_e^2$. P_e is the excitation power, $D_i = k_i/\rho_i c_{pi}$ is the thermal diffusivity, k_i is the thermal conductivity, ρ_i is the mass density, c_{pi} is the specific heat, t is the time, R is the reflectivity at the excitation wavelength, and w_e is the radius ($1/e^2$ in intensity) of the excitation beam on the surface of the sample. ϕ accounts for the fraction of the absorbed energy converted to heat; $\phi = 1$ if the absorbed energy is totally converted to heat. The deposition of thermal energy by light absorption is assumed to occur only at the surface of the sample, which can be represented in the high absorption limit by a Dirac delta function $Q(z) = 2\delta(z)$, bringing mathematical simplicity to the model.

The temperature gradients in the fluid and in the sample can be written in terms of the inverse of Laplace and Hankel transforms as

$$T_i(r,z,t) = \int_0^\infty T_i(\alpha,z,t) J_0(\alpha r) \alpha \mathrm{d}\alpha, \tag{2}$$

Optics EXPRESS

using the convolution theorem

$$T_i(\alpha, z, t) = \frac{k_s Q_0 Q(\alpha)}{\sqrt{D_s/D_f}} \int_{t_0}^{t} G(\alpha, t-\tau) H(\alpha, \tau, D_i) \mathrm{d}\tau, \tag{3}$$

in which $G(\alpha, t)$ and $H(\alpha, t, D_i)$ are given by the inverse Laplace transform of $G(\alpha, s)$ and $H(\alpha, s, D_i)$, respectively, as $H(\alpha, t, D_i) = \delta(t)$, for $z = 0$, $H(\alpha, t, D_i) = |z|(4\pi t^3 D_i)^{-1/2} \exp[-D_i\alpha^2 t - z^2/(4D_i t)]$, for $z \neq 0$, and

$$\begin{aligned} G(\alpha, t) = {} & \frac{k_s\sqrt{D_f}}{\alpha\kappa(k_s^2 D_f - k_f^2 D_s)} \left[\sqrt{D_s}\mathrm{erf}(\alpha\sqrt{D_s}\sqrt{t}) - e^{-\alpha^2\kappa t}\sqrt{D_s-\kappa}\mathrm{erf}(\alpha\sqrt{D_s-\kappa}\sqrt{t})\right] - \\ & \frac{k_f\sqrt{D_s}}{\alpha\kappa(k_s^2 D_f - k_f^2 D_s)} \left[\sqrt{D_f}\mathrm{erf}(\alpha\sqrt{D_f}\sqrt{t}) - e^{-\alpha^2\kappa t}\sqrt{D_f-\kappa}\mathrm{erf}(\alpha\sqrt{D_f-\kappa}\sqrt{t})\right]. \end{aligned} \tag{4}$$

Here, $\kappa = (k_s^2 - k_f^2)D_s D_f/(k_s^2 D_f - k_f^2 D_s)$, $\mathrm{erf}(x)$ is the error function, $J_0(x)$ is the Bessel function of the first kind and the Hankel transform of $Q(r)$ is $Q(\alpha) = (w_e^2/4)\exp(-w_e^2\alpha^2/8)$. $t_0 = 0$ accounts for the laser-on ($t<\xi$) and $t_0 = t - \xi$ for the laser-off ($t>\xi$) excitation regimes. ξ is the duration of illumination. Both excitation and relaxation regimes are recorded experimentally.

The temperature field is used then, as the source to compute the thermoelastic displacement of the sample, by solving the thermoelastic equation of motion with the appropriate initial and boundary conditions. The displacement field $\mathbf{u} \equiv \vec{u}(r, z, t)$ of a homogeneous and isotropic solid is given by the solution of [9]

$$(\lambda + 2\mu)\nabla^2\mathbf{u} + (\lambda+\mu)\nabla(\nabla\cdot\mathbf{u}) = \gamma\nabla T_s(r, z, t) + \rho_s\frac{\partial^2\mathbf{u}}{\partial t^2}, \tag{5}$$

where $\gamma = (3\lambda + 2\mu)\alpha_T$. $\lambda = E\nu_s/[(1+\nu_s)(1-2\nu_s)]$ and $\mu = E/2(1+\nu_s)$ are the Lame's constants, E is the Young's modulus, α_T is the linear thermal expansion coefficient, and ν_s is the Poisson's ratio of the sample. The last term on the right-hand side of the thermoelastic equation represents the inertia term yielding elastic wave motion. This term can be neglected [22] as the signal oscillations due to the inertia term are not observed experimentally considering the relatively long detector response time [23]. The z-component (normal) of the displacement vector at the sample surface for a semi-infinite sample is

$$\begin{aligned} u_z(r, 0, t) = {} & \theta_{\mathrm{TM}}\frac{\lambda_p k_s D_s\sqrt{D_f}}{\pi}\int_0^\infty\int_{t_0}^{t} \\ & \left[\frac{e^{-D_s\alpha^2\tau}}{\alpha\sqrt{\tau\pi}} - \sqrt{D_s}\mathrm{erfc}(\alpha\sqrt{\tau D_s})\right] G(\alpha, t-\tau)\alpha^2 e^{-w_e^2\alpha^2/8} J_0(\alpha r)\mathrm{d}\tau\mathrm{d}\alpha. \end{aligned} \tag{6}$$

$\theta_{\mathrm{TM}} = -P_e(1-R)(1+\nu_s)\alpha_T\phi/(k_s\lambda_p)$ [8] and λ_p is the probe beam wavelength.

The normal surface deformation given by Eq. (6) can be concurrently measured by the TM and the interferometer. The TM detection is performed by analyzing the on-axis intensity change of the central portion of the probe beam reflected from the sample surface at the far field photodetector [11,22]. The centers of both the pump and the probe beams overlap at the sample surface. The thermoelastic displacement created at the surface acts as a dynamic optical element to the wavefront of the probe beam increasing or diminishing its power passing the pinhole at the detector plane. $u_z(r, 0, t)$ produces a phase shift to the reflected portion of the TM probe beam

$$\Phi_{\mathrm{TM}}^s(r, t) = \frac{4\pi}{\lambda_p}u_z(r, 0, t). \tag{7}$$

Optics EXPRESS

Additional phase shift to the probe beam as a consequence of the thermal lens (TL) effect created in the surrounding air by heat coupling to the sample is given by [22]

$$\Phi^{f}_{\mathrm{TL}}(r,t) = \frac{4\pi}{\lambda_p}\left(\frac{dn}{dT}\right)_f \int_{-\infty}^{0}\left[T_f(r,z,t) - T_f(0,z,t)\right]\mathrm{d}z. \tag{8}$$

$(dn/dT)_f$ is the temperature coefficient of the fluid refractive index at λ_p. The probe beam wavefront distortion caused by the thermoelastic displacement of the sample and temperature change in the air is

$$\Phi_{\mathrm{TM}}(r,t) = \Phi^{s}_{\mathrm{TM}}(r,t) + \Phi^{f}_{\mathrm{TL}}(r,t). \tag{9}$$

The intensity of the reflected TM probe beam varies as [2]

$$S(t) = \left|\int_0^{\infty} \frac{2r}{w_p^2}\exp\left[-\left(1 + i\frac{z_1}{z_c}\right)\frac{r^2}{w_p^2} - i\,\Phi_{\mathrm{TM}}(r,t)\right]\mathrm{d}r\right|^2, \tag{10}$$

where z_c is the confocal distance of the probe beam, z_1 is the distance from the probe beam waist to the sample, and w_p is the radius of the probe beam at the sample surface. Equation (10) can be evaluated numerically using the calculated $u_z(r,0,t)$ and $T(r,z,t)$.

The total phase shift $\Phi_{\mathrm{TM}}(r,t)$ is sensed by both the photothermal mirror and the interferometer. The interferometer gives direct access to the phase shift at a chosen off-axis distance r while the photothermal mirror shows a convoluted signal resulting from the total phase shift at the sample surface and in the air given by Eq. (10). The physical parameters of the sample and fluid in $\Phi_{\mathrm{TM}}(r,t)$ can be rearranged in terms of θ_{TM}.

3. Experimental

The combined photothermal mirror and interferometer experiments use the pump-probe configuration schematically shown in Fig. 1. A cw excitation, a TEM_{00} optically pumped semiconductor laser (Coherent, Verdi G7, 532 nm), was used to pump the samples. The excitation laser is arranged almost collinear to both probe laser beams. The angles between each beam and the normal to the surface of the sample is always <1°. The exposure time of the sample to the excitation laser beam (laser-on and laser-off) is controlled by a mechanical shutter (SRS, Model SR470) with an oppening/closing time of about 6 μs. TM detection uses a He-Ne laser at 632.8 nm (Thorlabs, Model HNL225R-JP, 22.5 mW). The intensity variation of the probe beam center after reflection was detected by a pinhole-laser line filter-photodetector assembly PD(PTM)(Thorlabs, Model PDA36A2) in the far field. A digital oscilloscope (Tektronix, Model DPO 4102B) triggered by the photodiode PD(Trigger) (Thorlabs, Model PDA36A2) recorded the data. The measured decreasing/increasing intensity signal corresponds to the laser induced convex/concave optical element.

The interferometer uses a stabilized He-Ne laser at 632.8 nm (Thorlabs, Model HRS015B, 1.2 mW). The linearly polarized beam exiting the laser lies in the plane of the optical table (x–z plane). After the optical Faraday isolator (OFI), the beam polarization forms a 45° angle with respect to the x–axis. This polarization can be decomposed into two orthogonal polarizations with equal intensities, one in the plane of the paper (x–axis) and the other perpendicular to it (y–axis). The 50%–50% nonpolarizing cube beam splitter (NBS) evenly divides the beam into the reference and the measurement arm. The first transition through the $\lambda/8$, which is placed in the reference arm, gives rise to the 45° phase difference between the orthogonal polarizations. The beam is then reflected from the reference mirror ($\mathrm{M_{PZT}}$), which is driven by a piezoelectric transducer (PZT), and an additional 45° is added on the returning passage through the $\lambda/8$. The orthogonal polarizations in the measurement arm undergo an equal phase shift due to the displacement of the sample surface and the thermal lens generated in the surrounding air. The

Optics EXPRESS

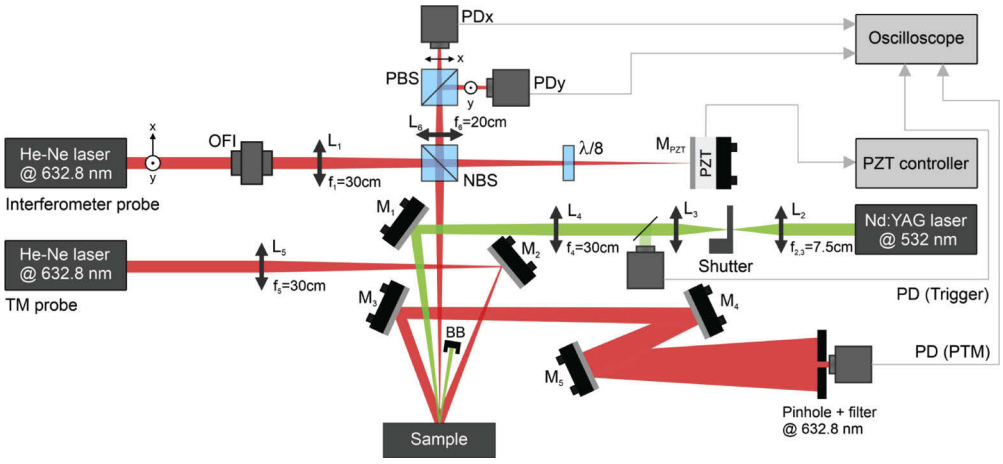

Fig. 1. Experimental diagram for the TM and the interferometer measurements. The pump and the probe beams are focused by the biconvex lenses L_j of focal lengths f_j. M_j, BB, and PD_j stand for mirrors, beam blocker, and photodiodes, respectively. NBS/PBS are the nonpolarizing/polarizing beam splitters, OFI is the optical Faraday isolator, $\lambda/8$ is the octadic wave plate and PDx,y detects the beam having x,y-polarization. The laser beams have radii: $w_e = 646$ μm, $w_p = 1584$ μm, $w_{\text{interf.}} = 154$ μm, at the surface of the sample. The experimental parameters are $z_c = 0.50$ cm, and $z_1 = 26.1$ cm. The temperature of the samples was 298 K.

polarizing beam splitter (PBS) transmits the x–polarization and reflects the y–polarization. The two beams with polarizations in the x–z/y–z plane, one from the reference arm and the other from the measurement arm, reach the Si photodiode PDx/PDy. The two photodiodes are equal and have equal amplification gains. Furthermore, the arms are of equal length so that the interfering beams have the same wavefront curvature. Ideally, the interference signals on the photodiodes are shifted by 90°, which can be achieved with a properly rotated $\lambda/8$. The measured time dependent phase shift due to the surface displacement and thermal lens in the air is encoded in the phase $\Phi_{\text{TM}}(r,t)$. The interferometer probes the phase at a position r by placing a lens just before the NBS to focus the probe beam, reducing the probing area, with radius $w_{\text{interf.}} = 154$ μm, at the surface of the sample. The phase shift is derived from the intensities I_x and I_y from the photodetectors PDx and PDy, respectively, and is given in terms of the DC offset I_0 as

$$\Phi_{\text{TM}}^{\text{int.}}(r,t) = \arctan\left[\frac{I_y(t) - I_0/4}{I_x(t) - I_0/4} + m\pi\right],\ m = 0, \pm 1, \ldots \tag{11}$$

The integer m must be chosen correctly, so that the function $\Phi_{\text{TM}}^{\text{int.}}(r,t)$ satisfies the condition of being continuous. As described in details in Ref. [24,25], the PZT was used to make a synthetic displacement of more than $\lambda/2$ in order to obtain the parameters of a full ellipse, which are used in the unwrapping process.

4. Results and Discussion

Experiments were performed in copper, bronze and inox cylinders having diameter of 50 mm and height of 15 mm. The samples were polished to obtain a mirror surface and irradiated by a focused laser beam. The results are presented in Fig. 2. The phase shift obtained from the interferometric measurements at $r = 0$, $\Phi_{\text{TM}}(0,t)$, was recovered from the unwrapping of the time-dependent signals from the photodiodes PDx and PDy – Fig. 2(a). Figure 2(b) shows the normalized intensity signal of the central portion of the TM probe beam, $S(t)/S(0)$. The signals

Optics EXPRESS

are averaged over 100 transients and the time interval between consecutive events is long enough for the sample to return to its unperturbed state.

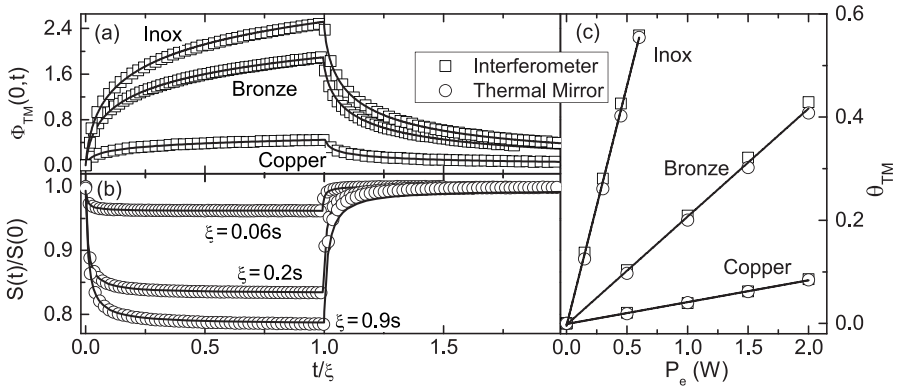

Fig. 2. Measured (open symbols) (a) interferometric and (b) TM signals for copper, bronze and inox as a function of the reduced time, t/ξ. Continuous lines represent the numerical fit of the experimental curves to $\Phi_{\rm TM}(0,t)$ (interferometer) and Eq. (10) (TM). (c) shows the retrieved $\theta_{\rm TM}$ from the interferometer (open squares) and the TM (open circles) as a function of the excitation power.

The surface deformation produced by the excitation laser acts as a convex mirror to the TM probe beam [26], decreasing the TM intensity signal at the photodetector at first, and then recovering it as the heat diffuses out of the irradiated region of the sample, reaching a steady state. The laser-off transients show the relaxation processes with the signal reaching the original values at $t = 0$. The interferometric transients, on the other hand, do not approach steady state for the excitation time used in this work as the phase shift continues to increase with time. The thermal diffusivity of the samples dictates how fast heat diffuses within the sample and out to the fluid, and the amplitude of the transients are related to the excitation power, thermal conductivities and thermal expansion coefficient of the sample.

The continuous lines in Figs. 2(a) and (b) are the numerical fit of the experimental curves to $\Phi_{\rm TM}(0,t)$ (interferometer) and $S(t)/S(0)$ (TM). Regression was performed by numerically evaluating these equations in a C++ compiled software. The data was fitted using a particle swarm optimization method where about a hundred different combinations of D_s and $\theta_{\rm TM}$ were evaluated and the global best result obtained. By performing another grid search around the global best fit we could confirm that the numerical confidence in the values are higher than 99%. The numerical fits are in good agreement with the measurements. The parameter $\theta_{\rm TM}$ recovered from both the interferometer and the TM measurements shows a linear dependence on the excitation power as displayed in Fig. 2(c). The linear regression gives $\theta_{\rm TM}/P_e$, which depends on the thermal conductivity of the sample. By using literature values for α_T and ν_s, and the measured reflectivity R, the results for k_s and $\rho_s c_{ps}$ are presented in Table 1. These results are in complete agreement with the literature values for the thermal and mechanical properties of the samples [27].

Even though TM and interferometer both measure the temporal dependence of the power of the probing light reaching the sensor, TM is more sensitive to the shape of the probed surface, while the two HQLI signals depend primarily on the phase shift induced by the displacement of the investigated surface. When both methods are compared, TM is superior for on-field measurements due to its practical insensitivity to mechanical vibrations and absolute surface displacement in the z–direction. On the other hand, the signal of the interferometer is easier to be fitted and is, assuming negligible contribution of the lens effect of the heated air, directly

Optics EXPRESS

Table 1. Physical properties of the metals. The literature values are for metals with characteristics similar to the samples investigated here. Reflectivity R is 0.58 for copper, 0.69 for bronze, and 0.60 for inox, and $(dn/dT)_{air} = -1 \times 10^{-6}\,K^{-1}$ [8].

Material	D_i (10^{-6}) m^2s^{-1}		θ_{TM}/P_e W^{-1}	k_i $Wm^{-1}K^{-1}$		$\rho_s c_{ps}$ (10^6) $Jm^{-3}K^{-1}$	ν_s	α_T (10^{-6}) K^{-1}
	This work	Ref. [27]	This work	This work	Ref. [27]	This work	Ref. [27]	Ref. [27]
Copper	105 ± 6	113	0.042 ± 0.001	355 ± 15	391	3.4 ± 0.2	0.31	17.3
Bronze	19 ± 2	17.6	0.210 ± 0.005	55 ± 3	59	2.9 ± 0.1	0.32	18.0
Inox	3.6 ± 0.1	4.0	0.93 ± 0.02	15.2 ± 0.7	16.2	4.2 ± 0.2	0.29	17.3
Air	21.9		0.026					

proportional to the z–component of the displacement and thus easily interpretable. If measured at different surface positions, mapping the excited region, the results from the interferometer can be used to reconstruct the surface bulging and thus validate the TM signal quantitatively. The unprecedented collective experimental power of using both methods at the same time not only cross validates each other, but also gives access to additional insights of the underlying physics, especially when the interferometer is used in the surface-scanning mode.

The combined interferometer/TM method presented here has applications for the characterization of opaque and even semitransparent materials. For semitransparent materials, light propagates and is absorbed within the sample and the effects following absorption must be considered in the theoretical description [28]. These methods are highly sensitive and non-contacting techniques. This makes the combined method a useful tool to investigate materials in a variety of environmental conditions by controlling temperature, pressure and even applying external electric and magnetic fields. Both methods are complementary in a sense that the interferometer is sensitive to the out-of-plane surface displacement of the sample at a single location, while the photothermal mirror reads a complex convolution of all the effects taking place in the sample surface and in the coupling fluid. TM has been proven to characterize laser induced thermoelastic waves generated locally and propagating within metals, thermo-optical and mechanical properties of semiconductors and semi-transparent materials, and even in detecting the effects of radiation pressure in dielectric liquids. The combination of the two techniques brings substantial improvements for single shot analysis and offer compelling support to describe the origins of light and mater interaction effects.

5. Conclusion

In summary, we proposed a combined photothermal mirror and interferometric detection method using simultaneous laser induced surface displacement to investigate thermal, optical and mechanical properties of metals. Both the wavefront distortion caused by the surface displacement of the sample and the thermal lens in coupling fluid are sensed by the probe beams from the two techniques. The combined technique gives direct access to the phase shift at a single location on the surface of the sample (interferometer) in addition to the convoluted signal arising from the total wavefront distortion in the media (photothermal mirror). Both methods are complementary in a sense that the interferometer is sensitive to the out-of-plane surface displacement of the sample at a single location, while the photothermal mirror reads a complex convolution of all the effects taking place on the sample surface and in the coupling fluid. The photothermal mirror has been proven to characterize laser induced thermoelastic waves generated locally and propagating within metals, thermo-optical and mechanical properties of semiconductors and semi-transparent materials, and even in detecting the effects of radiation pressure in dielectric liquids. The combination of the two techniques brings substantial improvements for single-shot analysis and offer compelling support to describe the origins of light and mater interaction effects.

Optics EXPRESS

Funding

Coordenação de Aperfeiçoamento de Pessoal de Nível Superior (Finance Code 001); Conselho Nacional de Desenvolvimento Científico e Tecnológico; Fundação Araucária; Javna Agencija za Raziskovalno Dejavnost RS (L2-9254, P2-0392).

Acknowledgments

This work is supported by Fundação Araucária, CAPES, and CNPq. The authors also acknowledge the financial support from the Slovenian Research Agency (P2-0392 and L2-9254).

Disclosures

The authors declare no conflicts of interest.

References

1. S. E. Bialkowski, N. G. C. Astrath, and M. A. Proskurnin, *Photothermal Spectroscopy Methods* (John Wiley & Sons, 2019).
2. L. C. Malacarne, F. Sato, P. R. B. Pedreira, A. C. Bento, R. S. Mendes, M. L. Baesso, N. G. C. Astrath, and J. Shen, "Nanoscale surface displacement detection in high absorbing solids by time-resolved thermal mirror," Appl. Phys. Lett. **92**(13), 131903 (2008).
3. Y. Shen and P. Hess, "Real-time detection of laser-induced transient gratings and surface acoustic wave pulses with a Michelson interferometer," J. Appl. Phys. **82**(10), 4758–4762 (1997).
4. V. Kurzmann. J. Stöhr, M. Tochtrop, and R. Kassing, "Interferometric measurement of thermal expansion," Mater. Sci. Eng., A **122**(1), 117–120 (1989).
5. S. A. Carp and V. Venugopalan, "Optoacoustic imaging based on the interferometric measurement of surface displacement," J. Biomed. Opt. **12**(6), 064001 (2007).
6. P. Beyersdorf and M. Cordier, "Measurement of thermo-elastic deformation of an optic using a polarization based shearing interferometer," Appl. Opt. **51**(31), 7426–7433 (2012).
7. G. Goetz, T. Ling, T. Gupta, S. Kang, J. Wang, P. D. Gregory, H. Park, and D. Palanker, "Interferometric mapping of material properties using thermal perturbation," Proc. Natl. Acad. Sci. **115**(11), E2499–E2508 (2018).
8. G. V. B. Lukasievicz, N. G. C. Astrath, L. C. Malacarne, L. S. Herculano, V. S. Zanuto, M. L. Baesso, and S. E. Bialkowski, "Pulsed-laser time-resolved thermal mirror technique in low absorbance homogeneous linear elastic materials," Appl. Spectrosc. **67**(10), 1111–1116 (2013).
9. O. A. Capeloto, G. V. B. Lukasievicz, V. S. Zanuto, L. S. Herculano, N. E. Souza Filho, A. Novatski, L. C. Malacarne, S. E. Bialkowski, M. L. Baesso, and N. G. C. Astrath, "Pulsed photothermal mirror technique: characterization of opaque materials," Appl. Opt. **53**(33), 7985–7991 (2014).
10. N. G. C. Astrath, G. V. B. Lukasievicz, L. C. Malacarne, and S. E. Bialkowski, "Surface deformation effects induced by radiation pressure and electrostriction forces in dielectric solids," Appl. Phys. Lett. **102**(23), 231903 (2013).
11. N. G. C. Astrath, L. C. Malacarne, M. L. Baesso, G. V. B. Lukasievicz, and S. E. Bialkowski, "Unravelling the effects of radiation forces in water," Nat. Commun. **5**(1), 4363 (2014).
12. O. A. Capeloto, V. S. Zanuto, L. C. Malacarne, M. L. Baesso, G. V. B. Lukasievicz, S. E. Bialkowski, and N. G. C. Astrath, "Quantitative assessment of radiation force effect at the dielectric air-liquid interface," Sci. Rep. **6**(1), 20515 (2016).
13. O. A. Capeloto, V. S. Zanuto, G. V. B. Lukasievicz, L. C. Malacarne, S. E. Bialkowski, T. Požar, and N. G. C. Astrath, "Generation and detection of thermoelastic waves in metals by a photothermal mirror method," Appl. Phys. Lett. **109**(19), 191908 (2016).
14. V. E. Gusev and A. A. Karabutov, *Laser optoacoustics* (American Institute of Physics, 1993).
15. C. B. Scruby and L. E. Drain, *Laser Ultrasonics, Techniques and Applications* (Adam Hilger, 1990).
16. R. Reibold and W. Molkenstruck, "Laser interferometer for ultrasonic applications," Acustica **49**, 205 (1981).
17. V. Greco, G. Molesini, and F. Quercioli, "Accurate polarization interferometer," Rev. Sci. Instrum. **66**(7), 3729–3734 (1995).
18. T. Požar, P. Gregorčič, and J. Možina, "A precise and wide-dynamic-range displacement-measuring homodyne quadrature laser interferometer," Appl. Phys. B **105**(3), 575–582 (2011).
19. T. Požar, J. Možina, and K. D. Sattler, in *Fundamentals of Picoscience* (Taylor and Francis, 2014), pp. 553.
20. T. Požar and J. Možina, "Mechanical wave motion due to the radiation pressure on gain or absorptive rods," Opt. Lett. **38**(10), 1754–1756 (2013).
21. J. Lazar, M. Holá, O. Číp, J. Hrabina, and J. Oulehla, "Interferometric system with tracking refractometry capability in the measuring axis," Meas. Sci. Technol. **24**(6), 067001 (2013).
22. G. V. B. Lukasievicz, L. C. Malacarne, N. G. C. Astrath, V. S. Zanuto, L. S. Herculano, and S. E. Bialkowski, "A theoretical and experimental study of time-resolved thermal mirror with non-absorbing heat-coupling fluids," Appl. Spectrosc. **66**(12), 1461–1467 (2012).

Optics EXPRESS

23. J. B. Spicer and D. H. Hurley, "Epicentral and near epicenter surface displacements on pulsed laser irradiated metallic surfaces," Appl. Phys. Lett. **68**(25), 3561–3563 (1996).
24. T. Požar and J. Možina, "Enhanced ellipse fitting in a two-detector homodyne quadrature laser interferometer," Meas. Sci. Technol. **22**(8), 085301 (2011).
25. P. Gregorčič, T. Požar, and J. Možina, "Quadrature phase-shift error analysis using a homodyne laser interferometer," Opt. Express **17**(18), 16322–16331 (2009).
26. L. Taylor and J. Talghader, "Monitoring and analysis of thermal deformation waves with a high-speed phase measurement system," Appl. Opt. **54**(30), 9010–9016 (2015).
27. J. W. Bray, P. Robinson, D. E. Tyler, and W. T. Black, *Metals Handbook: Properties and Selection: Nonferrous Alloys and Special-Purpose Materials*, v.2 (ASM International, 1990).
28. L. C. Malacarne, N. G. C. Astrath, G. V. B. Lukasievicz, E. K. Lenzi, M. L. Baesso, and S. E. Bialkowski, "Time-resolved thermal lens and thermal mirror spectroscopy with sample-fluid heat coupling: a complete model for material characterization," Appl. Spectrosc. **65**(1), 99–104 (2011).

193.2.78.34 {ts '2020-02-26 02:55:35'}